Proceedings of the
International Conference on Mechanical Engineering and Renewable Energy 2011
(ICMERE2011) 22- 24 December 2011, Chittagong, Bangladesh

ICMERE2011-PI-059

Fluid Flow Characteristics in S-Shaped Air Intake using Zero-Net-Mass-Flow

Mohammad Mashud and Md. Ilias Inam

Department of Mechanical Engineering
Khulna University of Engineering & Technology
Khulna-9203, Bangladesh
E-mail: kohel_11@yahoo.com

Abstract- *Flow control using zero-net-mass-flow jets in a two- dimensional model of an S-Shaped air intake diffuser was investigated. Experiments were conducted in a channel flow facility at a Reynolds Number of* $Re = 8 \times 10^4$ *with particular image velocimetry measurements in the symmetry plane of the duct. In the natural configuration, separation of the boundary layer occurs in a region of the duct with a high degree of curvature. A stability analysis of the wall normal profile at the location of the applied control is presented and estimates the most effective frequency of the actuator. Time-averaged velocity fields show total reattachment of the boundary layer using active flow control.*

1.INTRODUCTION

The complexity of modern aircraft enforces strong geometric constraints to the air inlets, which constitute the first element in the propulsive system. Today, industry commonly use air inlets with an "S" form, often with a restricted length. Some well known examples of aircraft that utilise S-shaped air inlets include the F16 and Eurofighter Typhoon. The proposal by Boeing for a sonic cruiser has the engines at the rear of a blended wing-body with S-shaped air inlet ducts supplying the compressor with air. One of the most significant drawbacks of such a geometry is the appearance of a separated boundary layer located in the curve, which causes decrease of the total pressure of the gas entering the compressor. Moreover, the strong curve is responsible for the development of a secondary flow composing of counter rotating vortices and responsible for flow distortions. Both aspects significantly degrade the performance of the propulsive system. Consequently, it is highly desirable to avoid boundary layer separation.

The design of engine inlets is one area where the prevention of flow separation may be significant in improving the over- all efficiency of the vehicle. One way to avoid the separation is to increase the inlet length hence reducing the pressure gradient. However, this strategy increases the size of the overall vehicle [11]. For many military applications, the inlet geometry is also constrained by stealth requirements. For example, a serpentine inlet can be used to hide the line of sight to the compressor face [12] in order to reduce the infra-red signature.

Flow control techniques have received a great deal of interest in the last decade [6]. There are four major separation control strategies:

- tangential blowing to directly energise the low momentum region near the wall [17];
- wall suction [16] to remove the low-momentum region;
- vortex generators (VGs) in the form of vanes and bumps [10]; and
- forced excitation devices [18].

Tangential blowing and suction are very effective in controlling separation. However, these strategies require a high mass flux source, thus they are rarely used. VGs are one of the methods most investigated. Numerous configurations, shapes and sizes have been explored to control boundary layer separation [16].

The mechanism for reattachment as suggested by these studies is that VGs produce strong vortices, which enhance the mixing between the high-momentum core flow and the low-momentum boundary-layer flow, thus energising the boundary layer fluid. However, VGs are a passive control strategy which is somewhat limited; they are fixed and can be optimised (location, size, and other parameters) for specific operating conditions. In addition, they generate an associated parasitic drag.

Unsteady flow control techniques have received more attention recently and have been shown to be quite effective in controlling separation [14]. Among these methods, synthetics microjets have shown some benefits [1] . Active flow control using arrays of fluidic actuators based on synthetic jet technology – previously demonstrated on external flows – have been successfully applied to internal flows by Amitay M. *et al.* [1] in diffusers. Synthetic jet actuators were placed within a region of a separated flow in a diffuser, leading to flow reattachment. It is noteworthy that jets can lead to flow reattachment even though they are placed downstream the separation of point.

Zero-Net-Mass-Flow (ZNMF) jets are created from the working fluid of the flow in which they are deployed. Linear momentum is transfered from the actuator to the fluid without net mass injection. Thus, these type of actuators have some interesting benefits in flow control, as no additional mass flow is required. The ZNMF jets are produced by an oscillating pres- sure in a cavity. This oscillating pressure creates a phase of blowing and a phase of suction through the sharp edges orifice of the cavity. In the case of a round jet, the ZNMF jets are formed of vortex rings during the phase of blowing. These rings move sufficiently far from the orifice by their self-induced velocity during the blowing phase to be mostly unaffected by the following suction phase. During the suction phase, ambient fluid is entrained into the cavity. More details about the ZNMF jets formation are available in the work of Cater and Soria [2]. Smith and Glezer [19] have proposed a schematic of the formation and action of such jets, shown in Fig. 1.

The characterisation of ZNMF jets is more difficult than for classical jets. All conventional parameters used in classical jets including mean velocity and hence Reynolds number based on mean velocity are equal to zero. Nevertheless, some parameters can be defined, such as the excitation frequency and the oscillatory momentum blowing coefficient. The oscillation frequency

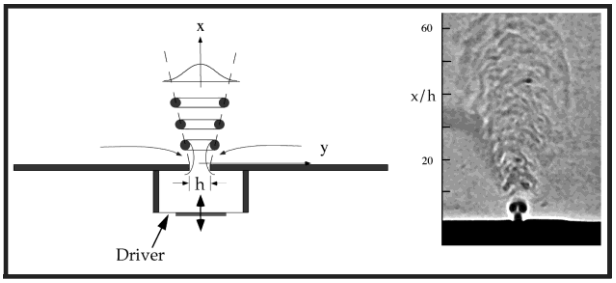

Figure 1: Schematic of ZNMF jet formation (Smith and Glezer [19]).

of the cavity, f, can be non-dimensionalised into the Strouhal number

$$St = \frac{fD}{U_{j,rms}} \quad (1)$$

where $U_{j,rms}$ is the rms velocity and D is the diameter of the ZNMF jets. The oscillatory momentum blowing coefficient is defined by the characteristic momentum imparted on the flow system by the jet, J, normalised by the characteristic momentum of the freestream qh (where h is the section of the freestream by unit length, and q the dynamic pressure);

$$C_\mu = \frac{J}{qh} = 2\frac{e}{h}\left(\frac{U_{j,rms}}{U}\right)^2 \quad (2)$$

where e is the equivalent thickness of the ZNMF jets.

In the case of a row of circular ZNMF jets, a third parameter P/D, is used as defined in Fig. 2.

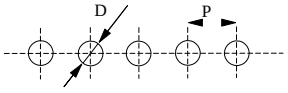

Figure 2: Definition of pitch and diameter for a row of circular ZNMF jets.

The effect of the ratio P/D on the development of ZNMF jets has received some interest in recent years, experimentally (Watson *et al.* [26, 27], Smith and Glezer [19]) and numerically (Guo and Kral [7]). From these studies, three modes of development were distinguished in the case of the interaction of two ZNMF jets:

- $P/D > 3$: the spacing is sufficiently large and the ZNMF jets are unaffected by the other one;
- $2 < P/D < 3$: the jets alter their trajectory and move towards one another; and
- $P/D < 2$: the jets almost combine immediately into a single and larger jet.

Nevertheless, all of the above studies were restricted to the interaction of two ZNMF jets. In the case of a row of jets some secondary effects can appear. In the present paper, it is not intended to analyse the interaction of the ZNMF jets, but to extend their application in a somewhat unexplored configuration of flow control (a ratio P/D greater than 3 will be used). Thus, the present work proposes the investigation of the capabilities of ZNMF jets in separation control in internal flow with strong curvature, such as an S-shaped air intake diffuser.

2.EXPERIMENTAL MODEL

2.1 Facility and Model

The experiments were conducted in a subsonic open channel flow at Monash University. This facility has a centreline velocity range from 1 to 35 m/s, with a working test section of $1 \times 0.85 \times 0.2$ m ($W \times L \times H$). Honeycomb filters and six screens in the settling chamber ensure the uniformity of the flow. The contraction following the settling chamber has a ratio of 1:10. A 2.6 m long channel of aspect ratio 1:10 beyond the contraction ensures a fully turbulent boundary layer at the enter of the working section (Tab. 1). The experiments were conducted at a centreline velocity of $U_c = 12.4$ m/s, corresponding to a Reynolds number at the S-shaped leading edge of about

$Re = U_c h_1 / \quad = 8 \times 10^4$ (where $h_1 = 98$ mm is the inlet height of the S-duct defined hereafter).

Re_x	$/h_1$	$^*/h_1$	$/h_1$	H
2×10^6	0.81	0.15	0.10	1.44

Table 1: Boundary layer characteristics at the enter of the test section (Re_x is the local Reynolds number based on the distance of the channel from the contraction to the inlet section, 2.6 m, and the centreline velocity U_c).

Throughout this paper, the coordinate system, x, y and z, refers to the streamwise, normal and spanwise directions, with respective velocity components are denoted by u, v and w. The origin is set on the symmetry plane of the duct, the inlet section and the bottom wall. A curvilinear coordinate system x_s and y_s is also used to describe the flow following the curved surface of the duct (z is unchanged, as the model is two-dimensional). Overbars indicate time-averaged values and the superscript " ' " is used to denote fluctuating components.

The geometry used for the test model is a simple two-dimensional representation of the test case used by Vuillerme *et al.* [25]. Its geometry is represented in Fig. 3.

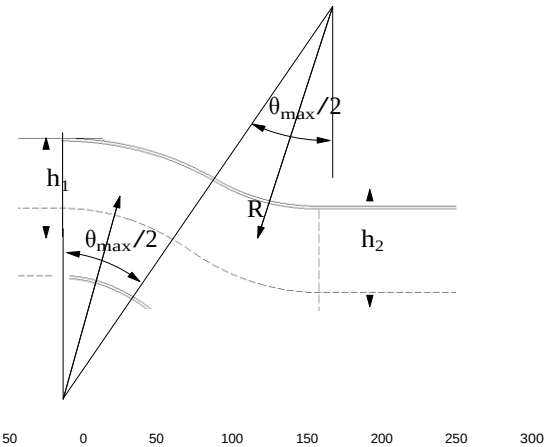

Figure 3: Geometry of the S-shaped air intake model.

ICMERE2011-PI-059

The duct centreline is defined by two arcs with $_{max}/2 = 30^{\circ}$ and an identical radius of curvature $R = 228.4$ mm. The (x_c, y_c) coordinates of the duct centreline, in Cartesian coordinates, are given by Eq. 3 to 6.

For $0 \leq \leq {}_{max}/2$:

$$x_c = R\sin(\ ) \tag{3}$$
$$y_c = R\cos(\ ) - R \tag{4}$$

For ${}_{max}/2 \leq \leq {}_{max}$:

$$x_c = 2R\sin(\ {}^{max}_{2}\ ) - R\sin(\ {}_{max} - \ ) \tag{5}$$
$$y_c = 2R\cos(\ {}^{max}_{2}\ ) - R\cos(\ {}_{max} - \ ) - R \tag{6}$$

The height h of the cross-section perpendicular to the centreline varies with the arc angle , and is given by

$$\frac{2h}{h_1} = 1 + 3\left(\frac{h_2}{h_1} - 1\right)\left(\frac{}{}_{max}\right)^2 - 2\left(\frac{h_2}{h_1} - 1\right)\left(\frac{}{}_{max}\right)^3 \tag{7}$$

where h_1 and h_2 are respectively the inlet and outlet height of the duct. The values used for construction are $h_1 = 98$ mm and $h_2 = 121.5$ mm, which provides an area ratio of 1.24. The vertical offset of the duct resulting from centreline curvature is $H = 0.62h_1$ and the length of the duct is $L = 1.88h_1$. This gives a ratio of step height to length $H/L = 0.25$.

Active flow control was realised using a row of ZNMF jets. The geometry repartition of the ZNMF jets was chosen according to the work of Soria and Stephens [24], studying the capacity of such a series actuators to enhance the lift of an aerofoil at a high angle of attack. The ratio $P/D = 6$ was retained, as it corresponded to the greatest capacity of the ZNMF jets to promote flow reattachment. The ZNMF jets have a round section diameter of $D = 0.5$ mm with a pitch $P = 3$ mm ($D/ = 0.013$, $D/ = 0.095$). They are disposed in a row of $W_c = 500$ mm in the spanwise direction, centred around the symmetry plane of the duct. This corresponds to the semi-spanwise dimension of the channel ($W = 1000$ mm), sufficiently far from the side walls to avoid any side effect (the study is limited here to the symmetry plane of the duct). Moreover, five identical rows of jets were mounted in the concave (bottom) wall of the duct. These rows are located from $s/L_s = 0.1$ to 0.5, with a spacing of 0.1 (in curvilinear coordinates). A scheme of the wall-mounted rows of ZNMF jets is given in Fig. 4, and a view of the model and the rows of ZNMF jets, mounted in the channel flow facility is shown in Fig. 5.

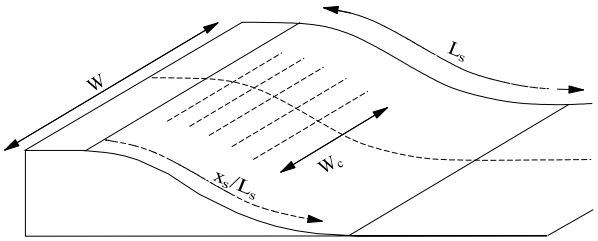

Figure 4: Schematic view of the rows of ZNMF jets.

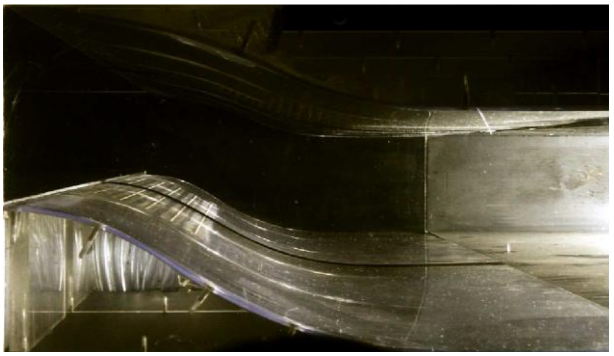

Figure 5: View of the S-shaped air intake model and ZNMF rows mounted in wind tunnel.

2.2 Measurement Technique

Particle Image Velocimetry (PIV) measurements were performed in this investigation to capture the velocity field. The channel flow was seeded with atomised olive oil particles, with typical diameter of less than 1 μm. A dual cavity Nd:YAG laser was used to generate the laser sheet, of about 1 mm thickness and aligned with the symmetry plane of the duct (Fig. 6). The laser sheet emission was driven at 0.35 Hz and synchronised with an high resolution PCO.4000 camera, in single-exposure and double image mode.

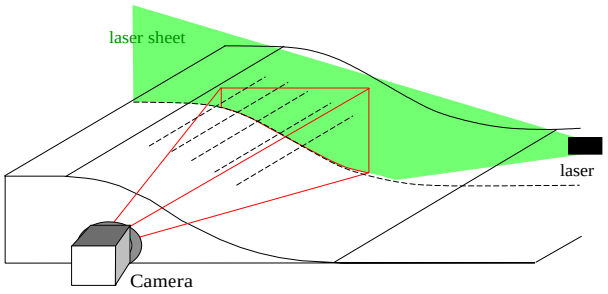

Figure 6: PIV set-up.

The camera resolution is 4008 × 2672 coupled with a 105 mm focal lens, giving a spatial resolution of 37.33 μm/pixel and image frame with dimension $1.5h_1 \times h_1$. The region of interest captured by the PIV measurements is schemed in Fig. 7. These single exposed image pairs were analysed using the multi-grid cross-correlation digital PIV (MCCDPIV) algorithm described in [21, 23]. Details of the performance, precision and experi- mental uncertainty of the MCCDPIV algorithm with applica- tions to the analysis of single exposed PIV and holographic PIV (HPIV) images have been reported in [22, 5], respectively.

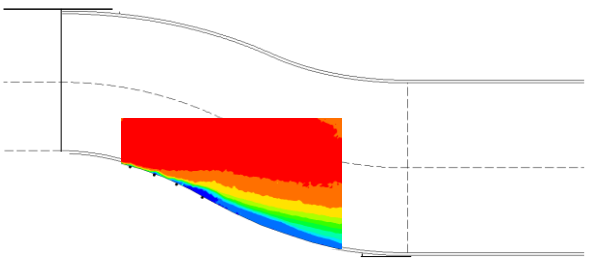

Figure 7: Scheme of the region of interest captured by PIV measurements.

3.RESULTS AND DISCUSSION

3.1 Uncontrolled Flow

The analysis of the natural flow inside the intake was investigated. A review of the natural flow condition determined the control parameters for the ZNMF jets. The jet position along the wall was selected to be as close upstream to the steady separation point as possible.

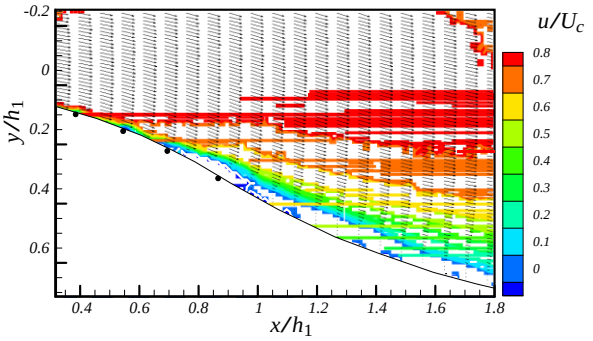

Figure 8: Mean velocity field for the natural flow conditions – contours represent the streamwise velocity component and vectors represent the vector field (u, v) – the white line indicates the zero velocity – white body represents the bottom wall of the duct and black points show the location of the 2nd to 5th rows of ZNMF jets.

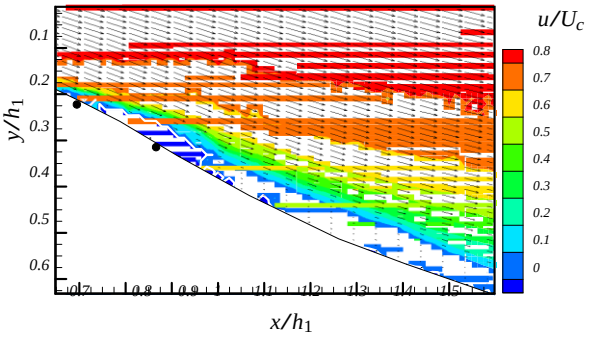

Figure 9: Mean velocity field for the natural flow conditions, zoom around the separation region – contours represent the streamwise velocity component and vectors represent the vector field (u, v) – the white line indicates the zero velocity – white body represents the bottom wall of the duct and black points show the location of the 2nd to 5th rows of ZNMF jets.

The velocity field, obtained using the PIV, is shown in Fig. 8 & 9. In these figures, contours of the non-dimensional mean streamwise velocity component u/U_c are plotted, and superimposed with velocity profiles (u, v). It appears that local separation of the boundary layer occurs where the curvature is a maximum. It is noteworthy that reverse flow is not clearly observed inside the separation region. This is due to surface reflections

from the Nd-YAG laser, inducing a low PIV correlation in this region. This could not be overcome with mean image subtraction due to the signal-noise ratio in this region. The rejected vectors have been replaced by zero values. However, the boundaries of the separation region appear clearly (white line). The separation has an extent of about $0.2h_1$, and induces strong effects on all profiles downstream (Fig. 9). Indeed, downstream of the separation region, wake profiles can be seen up to the end of the measurement window. The point of separation is located between the 4th and the 5th row of ZNMF jets, at about $x/h_1 = 0.75$. Based on this result, the 4th row of ZNMF jets ($x/h_1 = 0.72$) is used for the controlled experiments as a first approach (currently, only one set of control parameters has been studied).

The desired effect of active flow control will be to reduce the separation using the row of ZNMF jets chosen here. The next section is devoted to the stability analysis of the natural velocity field presented above, in order to determine the most spatially unstable frequency. This frequency is expected to achieve the strongest effect on downstream flow separation reduction.

3.1.1 Mapping of Orr-Sommerfield Squire Equations

A linear local stability analysis was undertaken on the mean velocity field. The stability of a fluidic system is governed by the perturbation form of the *Navier-Stokes Equations* (NSE) to determine the effect that small perturbations have on the transition to turbulence. The perturbation form of the NSE is formed by substituting the Reynolds' decomposition of velocity ($\mathbf{u} = \bar{\mathbf{u}} + \tilde{\mathbf{u}}$) and pressure ($p = \bar{p} + \tilde{p}$) into the NSE and expand- ing the terms. The *over-bar* modifier designates the time aver-
aged mean and the *tilde* a small fluctuating component. A system is unstable if this fluctuating component grows in both time and space. Assuming the mean component is not time varying, then the NSE of only the mean terms are then subtracted away. The non-linear components are assumed to be negligible in the early stages of growth of the instabilities. Assuming the mean velocity field is parallel, then only the wall tangential velocity $\bar{u}$ is non-zero, and a function of only the wall normal direction y. Substituting this mean field form into the perturbation form of the NSE the *Orr-Sommerfeld Equations* (OSE) results [15, 20]. The OSE are posed as a generalised eigenvalue problem as follows:

$$i \quad A\tilde{v} = B\tilde{v} \tag{8}$$

$$i \quad {}^{2}\tilde{v} = (-ik_{x_s}\bar{u} \quad {}^{2} + ik_{x_s} \quad {}^{2}\bar{u} + \frac{1}{Re} \quad {}^{4})\tilde{v} \tag{9}$$

where $\equiv (ik_{x_s}, \ _{y_s}, ik_y)$. Hence $^2 \equiv \ ^2_{y_s^2} - k^2 I$ and $^4 \equiv \ ^4_{y^4_s} - 2k^2 I + k^4 I$, where $k^2 \equiv k^2_{x_s} + k^2_z$ and I is the identity matrix. The perturbation component of the wall normal velocity $\tilde{v}$ is related to its eigenvectors $\hat{v}$ and associated temporal eigenvalues by

$$\tilde{v}(x_s, y_s, z, t) = \hat{v}(y_s)e^{ik_{x_s}x_s + ik_z z - i \ t} + c.c. \tag{10}$$

where k_{x_s} and k_z are the complex wave-numbers in the wall tangential direction (x) and the spanwise direction (z) respec- tively, and *c.c.* the complex conjugate of the first term. For the
present study $k_z = 0$, as within the OSE framework the most unstable eigenvalue for a given system will always occur for this particular spanwise wavenumber [4]. The system is also non-dimensionalised with respect to the centreline velocity U_c and the tunnel height at the inlet h_1. The code used to solve the generalised eigenvalue problem in equation 8 is discretised in y, using a spectral Chebyshev collocation method. The *Chebyshev* derivative matrices $D^{(n)}$ replace the $^n_{y_s^n}$ operators applied to the perturbation components. The code is written in *C++*, utilising the *Blitz++* library to handle the complex number mathematics and matrix operations, and *clapack* for the eigenvalue calculations.
The spatial resolution necessary for the stability analysis is greater than that available from the PIV measurements, consequently interpolation of the data is required. For each point on

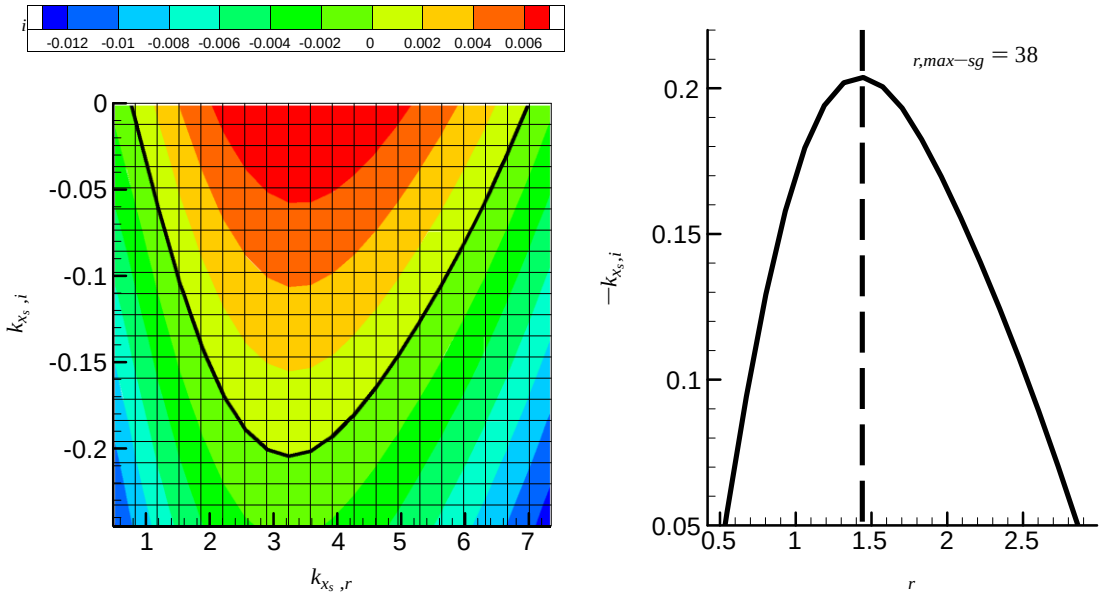

Figure 10: Mapping of Orr-Sommerfeld Squire equations for the velocity profile immediately prior to the point of separation: (a) contours of $_i$ plotted on the complex k_{x_s} plane with the line $_i = 0$; (b) determining frequency of maximum spatial growth.

the velocity profile, a two-dimensional (2-D) polynomial least squares error surface is fit to the PIV measurements and used to interpolate the mean velocity field. The number of points required to reconstruct the surface (m) is

$$m = \frac{1}{2}(n+1)(n+2) + p, \qquad (11)$$

where p the number of additional redundant points included in the least squares minimisation, above what is necessary to define a surface of order n [3]. The stencil of m data points from the PIV measurements utilised to fit the polynomial surface is selected on the basis of proximity to the position on the velocity profile required for interpolation. A Gaussian function is also used to weight the value of each data point inversely proportional to its distance from the required point of interpolation. The second order Cartesian derivatives of the mean Cartesian velocities are analytically determined from this surface. $\frac{^2\bar{u}}{y_{2_s}}$ (where y_s is wall normal direction and not the Cartesian direction) is then reconstructed from these Cartesian second order derivatives.

The stability analysis is undertaken immediately downstream of the ZNMF jets used in the controlled experiment. The value of the most unstable eigenvalue at this position, was found to converge for a polynomial surface of $n = 5$ and a redundancy of $p = 6$, with 64 Chebyshev collocation points used to discretise the wall normal direction. These parameters are used for each of the simulations undertaken in the following mapping.

A series of unstable spatial wave numbers of varying growth rate ($k_{x_s,i}$) and period ($k_{x_s,r}$) are mapped to the temporal complex plane through the OSE[1]. For each grid point in Fig. 10(a) an eigenvalue problem is solved and the most unstable temporal eigenvalue identified. Each grid point is then coloured by the growth rate of this eigenvalue ($_i$). The thick black line indicates where $_i = 0$. This line is important as there is no tempo- ral growth and is representative of the ZNMF jets providing a perturbation at a constant amplitude. The temporal period ($_r$) for which the spatial growth is maximised is determined by in terpolating the values of $k_{x_s,i}$ onto the thick black line and plotting the result against the associated $_r$ – see Fig. 10(b). $k_{x_s,i}$ is negated as a perturbation is spatially unstable for $k_{x_s,i} < 0$. The maximum spatial growth occurs at $_{r,max-sg} = 1.43$, which is equivalent to a dimensionalised frequency $f_{r,max-sg}$ of

$$f_{r,max-sg} = \frac{1}{2}\frac{_{r,max-sg}U_c}{h_1} = \frac{1}{2}\frac{1.43 \times 12.4}{0.098} = 28.8Hz. \qquad (12)$$

The instability can also be classed as convective, as no pinch point was evident in the unstable region of the temporal complex plane, indicating that the disturbance can only travel downstream [9, 8].

3.2 Controlled Flow

The control is applied using the ZNMF jets closest to the time average separation point as possible. The stability analysis of the mean velocity field at this location allowed the determination of the most spatially unstable frequency. The other parameter for the ZNMF jets is the maximum velocity of the blowing phase $U_{j,rms}$. This parameter is a function of the frequency f of the actuator and of the displacement of the oscillating mechanism d (here generated by a piston)

$$U_{j,rms} = \sqrt{2}\,(A/A_j)(fd) \qquad (13)$$

where A is the section of the cavity and A_j is the equivalent section of the row of ZNMF jets. For the present study, a 4.5 mm displacement of the oscillating piston was chosen, which generates the oscillating pressure in the cavity. The amplitude is limited to the capability of the stepper motor and scotch yoke driving the piston. This leads to a maximum velocity of 5.4 m/s for the most unstable frequency of 28.8 Hz. All of the ZNMF

[1] For each complex number, the subscript i denotes the imaginary component, and subscript r the real component

jets parameters are summarised in Tab. 2. It should be noted that only very low energy ($C_\mu = 0.026\%$) is necessary for effective flow control.

Control location	St	$U_{j,rms}/U_c$	C_μ
$x/h_1 = 0.72$	0.0029	0.44	0.026%

Table 2: ZNMF jets setting.

The mean velocity field obtained with the control is given in Fig. 11. When the ZNMF jets are active, the separation region disappears totally. Moreover, the velocity profiles do not exhibit any wake component downstream of the control point. The velocity profile develops downstream without any separation, with a small region of deficit velocity, resulting from the adverse pressure gradient.

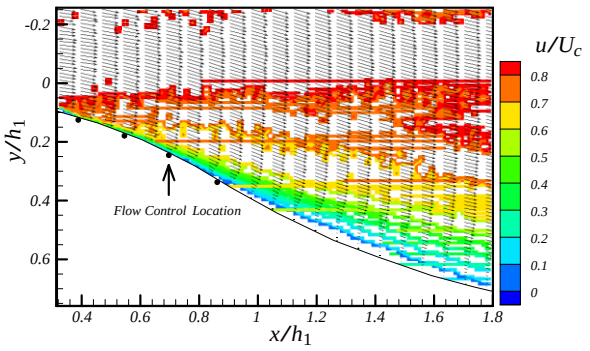

Figure 11: Mean velocity field for the controlled case – contours represent the streamwise velocity component and vectors represent the vector field (u, v) – white body represents the bottom wall of the duct and black points show the location of the 2nd to 5th rows of ZNMF jets.

4. CONCLUSIONS

Control of flow separation occurring in an S-shaped intake with strong curvature has been successfully realised using a row of ZNMF jets. Based on the analysis of the natural velocity field inside the intake, the most effective parameters for exciting the flow were determined.

The most effective frequency was identified as $St = 0.0029$ for the row of ZNMF jets directly upstream of the separation point. The results for the mean velocity field showed that the separation disappears completely using a row of ZNMF jets. However, these preliminary results are somewhat limited. Only a few parameters have been analysed, as there is additional PIV data for many other configurations of the control model. Through analysis of the turbulent field and large-scale structures of the flow (using a Proper Orthogonal Decomposition, for example), additional flow features could be extracted. Such information would be valuable, as it is of equal interest to reduce the level of turbulent distortion at the outlet of the duct, as well as reduce separation. To further understand the impact of the ZNMF jets on the flow and the mechanisms involved, phase-locked measurements with the oscillating pressure of the cavity of the ZNMF jets can also be undertaken. From this, information can be obtained regarding the blowing and suction phases of the jets' oscillation. In addition, the effects of changing different control parameters such as the frequency, *rms* velocity and the location of the ZNMF jets could also be explored. This will enable determination of the range of parameters for efficient flow control, and a more accurate determination of the control parameters inducing reattachment with the lowest input energy.

References

[1] Amitay, M., Pitt, D., Kibens, V., Parekh, D. and Glezer, A., Control of Internal Flow Separation Using Synthetic Jet Actuators, *AIAA paper 2000–0903*, 2000.

[2] Cater, J. E. and Soria, J., The Evolution of Round Zero-Net-Mass-Flux Jets, *J. Fluid Mech.*, **472**, 2002, 167–200.

[3] Chenoweth, S. K. M., Numerical simulation of wall jets, Confirmation report, Ph.D. thesis, University of Melbourne, 2007.

[4] Drazin, P. G. and Reid, W. H., Hydrodynamic stability, *Cambridge, New York: Cambridge University Press*, 1981.

[5] von Ellenrieder, K., Kostas, J. and, Soria J., Measurements of a wall-bounded, turbulent, separated flow using hpiv, *J. Turb.*, Special issue: 8th European Turbulence Conference, **2**, 2000, 1–15.

[6] Gad-el-Hak, M., and Bushnell, D. M., Separation Control: A Review, *J. Fluids Eng.*, **113**, 1991, 5-30.

[7] Guo, D. and Kral, L. D., Numerical simulation of the interaction of adjacent synthetic jet actuators, *AIAA paper 2000-2565*, 2000.

[8] Huerre, P. and Monkewitz, P. A., Absolute and convective instabilities in free shear layers, *J. Fluid Mech.*, **159**, 1985, 151–168.

[9] Kupfer, K., Bers, A. and Ram, A. K., The cusp map in the complex-frequency plane for absolute instabilities, *Phys. Fluids*, **30**, 1987, 3075–3082.

[10] Lin, J. C."Review of Research on Low Profile Vortex Generators to Control Boundary Layer Separation", *Progress in Aerospace Sciences*, **38 (4)**, 2002, 389–420.

[11] MacMartin, D. G., Verma, A., Murray, R. M., and Paduano, J. D., Active Control of Integrated Inlet/Compression Systems, *Fluids Eng. Div. Summer Meeting, FEDSM2001–18275*, 2001.

[12] Mayer, D. W., Anderson, B. H., and Johnson, T. A., 3D Subsonic Diffuser Design and Analysis, *AIAA Paper 98–3418*, 1998.

[13] Monkewitz, P. A. and Huerre P., Influence of the Velocity Ratio on the Spatial Instability of Mixing Layers, *Phys. Fluids*, **25 (7)**, 1983, 1137–1143.

[14] Nishri, B. and Wygnanski, I., Effects of periodic excitation on turbulent flow separation from a flap, *AIAA J.*, **36 (4)**, 1998, 547–556.

[15] Orr, W. M. F., The stability or instability of the steady motions of a perfect liquid and of a viscous liquid. part I: A perfect liquid; part ii: A viscous liquid, *Proc. R. Ir. Acad. A*, **27**, 1907, 9-68 and 69–138.

[16] Prandtl, L., Uber Flussigkeitsbewegung bei sehr kleiner Reibung, *Proc. of 3rd International Mathematical Congress*, Heidelberg, Teubner, Leipzig, Germany, 1905, 484–491.

[17] Schlichting, H., Boundary Layer Theory, 8th ed., Springer-Verlag, Berlin, 2000, 294–295.

Proceedings of the
International Conference on Mechanical Engineering and Renewable Energy 2011
(ICMERE2011) 22- 24 December 2011, Chittagong, Bangladesh

ICMERE2011-PI-059